

Double Refinement Network for Efficient Monocular Depth Estimation

Nikita Durasov¹, Mikhail Romanov¹, Valeriya Bubnova¹, Pavel Bogomolov¹, Anton Konushin¹

Abstract—Monocular depth estimation is the task of obtaining a measure of distance for each pixel using a single image. It is an important problem in computer vision and is usually solved using neural networks. Though recent works in this area have shown significant improvement in accuracy, the state-of-the-art methods tend to require massive amounts of memory and time to process an image. The main purpose of this work is to improve the performance of the latest solutions with no decrease in accuracy. To this end, we introduce the Double Refinement Network architecture. The proposed method achieves state-of-the-art results on the standard benchmark RGB-D dataset NYU Depth v2, while its frames per second rate is significantly higher (up to 18 times speedup per image at batch size 1) and the RAM usage per image is lower.

I. INTRODUCTION

In computer vision, depth estimation is the task of obtaining a measure of distance for each pixel of an image. It has a wide array of applications in consumer electronics (for example, in mobile photography) as well as in other computer vision tasks (simultaneous localization and mapping, visual odometry, to name a few). One of the most challenging settings in this field is monocular depth estimation, i.e. retrieving depth from a single image. Unlike other scenarios, such as stereo depth estimation, it does not require any additional equipment, and therefore can be applied in any devices with a camera, e.g. mobile phones, augmented reality headsets, indoor robots. In our work, we focus on monocular depth estimation exclusively.

We consider the regression problem of point-wise depth reconstruction. More specifically, we want to train a model $f(x): \mathbb{R}_{H \times W \times 3} \rightarrow \mathbb{R}_{H \times W \times 1}$ to predict the distance from the camera to the corresponding object for each pixel.

Recent approaches employ deep neural networks to solve this task and show significant improvements in quality over classical methods. However, their time and memory requirements for processing a single image are very high, which renders them unusable for production purposes, especially in portable devices. One of the most computationally expensive parts of these networks seems to be the bilinear interpolation of feature maps to the input size since the resulting tensor typically has very high dimensions. We propose a network architecture, called Double Refinement Network, which performs the interpolation iteratively while reducing the number of channels on each level. We evaluate our model on the standard benchmark RGB-D dataset NYU Depth v2 and show noticeable performance gain without compromising accuracy.

Firstly, we overview the recent work on the topic of monocular depth estimation. After that, we describe our architecture and experiments. Finally, we discuss the results and summarize our contribution.

II. RELATED WORK OVERVIEW

A. Classical methods

Depth estimation has been actively researched for over a decade. First methods did not rely on deep learning and instead utilized more algorithmic approaches.

Saxena et al. [22] used Markov Random Field to divide an image into superpixels, and reconstructed the 3D structure of the image by estimating the position and orientation of the 3D surfaces that the superpixels represented. Several geometry-based algorithms for indoor depth estimation including [9] and [5] were based on a number of assumptions about room shapes and the usual object placement in such rooms. [5] used SVM to compute a feature vector for each surface. [10] presented a system that modeled geometric classes depending on the orientation of a physical scene and built the geometric structure progressively. Geometry-based approaches worked with certain constraints and were relevant only for specific types of images.

B. Deep Learning Methods

Most recent works on depth reconstruction utilize Deep Convolutional Neural Networks (DCNN) [3], [14], [15], [16], [18]. It is common practice to use pre-trained layers (e.g. VGG [23], SENet [12] or ResNet [7]) for feature extraction. Another noticeable trend is exploiting encoder-decoder architectures. In such architectures, convolutional and max-pooling layers usually form the encoder and upsampling layers often play the role of the decoder. Here we overview some of the latest works with high benchmark results.

In [6] Gurram et al. propose a solution which includes training a model on two heterogeneous datasets, one with depth and the other with semantic map labels. Common NN layers are trained alternately on data from either of the datasets. In particular, the network consists of two flows that can be used for getting the depth or the semantic map of an image respectively.

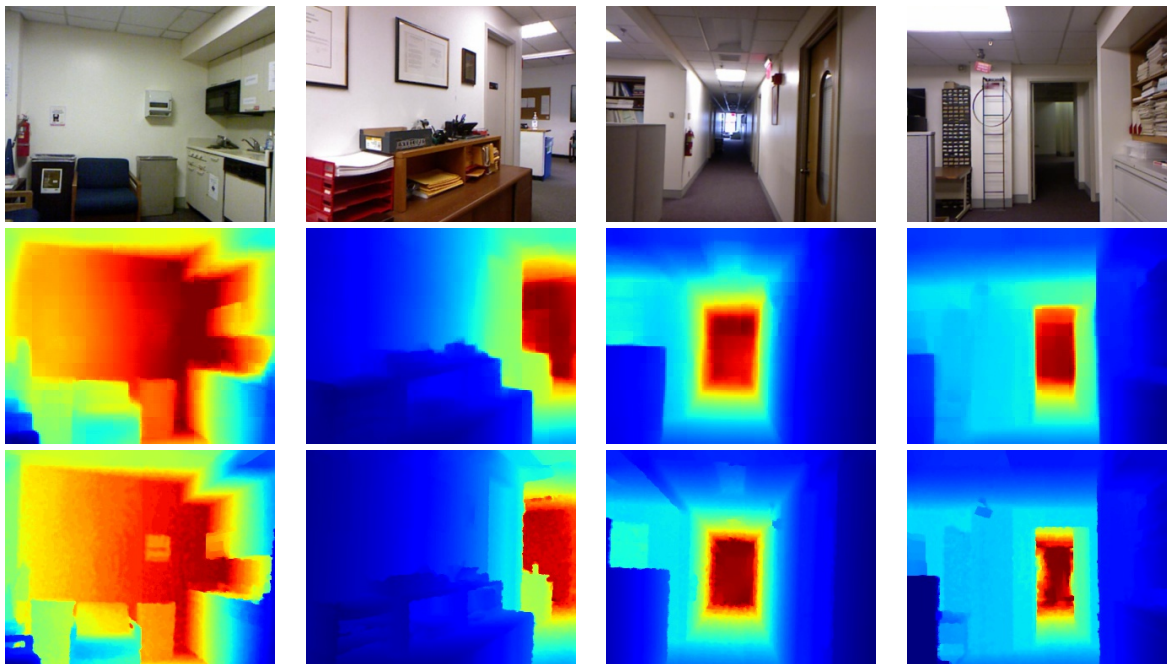
Fu et al. [4] formulate monocular depth estimation as an ordinal regression problem, i.e. they discretize depth. Their architecture includes a dense feature extractor (convolutions and dense layers), a scene understanding modular (a concatenation of dilated convolutions, a full-image encoder, and convolutional layers) and an ordinal regression block.

He et al. [8] make a point that without prior knowledge about the focal length of the camera, depth prediction can

¹Samsung AI Center Moscow, {n.durasov, m.romanov, v.bubnova, p.bogomolov, a.konushin}@samsung.com

TABLE I

NETWORK PREDICTIONS COMPARED TO THE GROUND TRUTH. FROM TOP TO BOTTOM: INPUT, NETWORK DEPTH MAP PREDICTION, GROUND TRUTH DEPTH MAP



be ambiguous. They suggest that using datasets with various focal lengths may be helpful in handling this issue. The proposed method involves generating multiple images with different focal lengths from one fixed-focal-length image. Thus, the model is trained on a varying-focal-length dataset. Focal lengths are given to the network in addition to images.

Spek et al. [24] train an encoder-decoder-solver architecture and approximate the encoder and decoder with their less computationally expensive versions. As a result, their architecture allows real-time depth estimation.

RefineNet [17] is a segmentation network which can also be used for depth estimation. It is similar to U-Net but is based on ResNet. One of its advantages is a high FPS rate compared to other state-of-the-art architectures.

Hu et al. [11] interpolate the ResNet feature maps of all the encoder layers to the size of the input and concatenate them. The resulting feature map is then passed into a custom decoder. This method, which we refer to as RSIDE, achieves state-of-the-art results and is the baseline for our work.

III. METHOD

We improve upon the baseline by making the following changes:

- Substitute bilinear interpolation of the feature maps to the size of the input with iterative pixel shuffle upsampling (in upI)
- Add another branch for intermediate depth maps (upII) with auxiliary losses applied to them

We call the resulting architecture Double Refinement Network. As we show further, this architecture is significantly

more computationally efficient than the baseline.

A. Relation to the State-of-the-Art Architectures

The current state-of-the-art architectures have high requirements for computational resources and memory. Some of the architectures (such as in [11]) use bilinear interpolation of all the deep activation maps to the input size. This procedure is very time- and memory-consuming, which leads to a low FPS rate.

PSPNet [26] and DeepLab v3 [1], [2], which can be applied to the depth estimation problem, use computationally expensive dilated convolutions.

In the proposed architecture, we replace dilated convolutions and bilinear interpolation of high-dimensional activation maps with iterative pixel shuffle upsampling. However, such changes may cause a decrease in accuracy.

To mitigate this, we propose a double-refinement framework. We start by obtaining a low-scale depth estimation, which we then iteratively improve, using the high-level backbone features. On each scale, we compute the correction term from the previous approximation and the lower-level backbone features. This requires less information and enables us to only upsample feature maps between consecutive levels, saving time and memory needed to interpolate them to the input size. We add this correction term to the upsampled depth estimation from the previous level, producing a new estimation at twice the resolution. The final output is of the same size as the input.

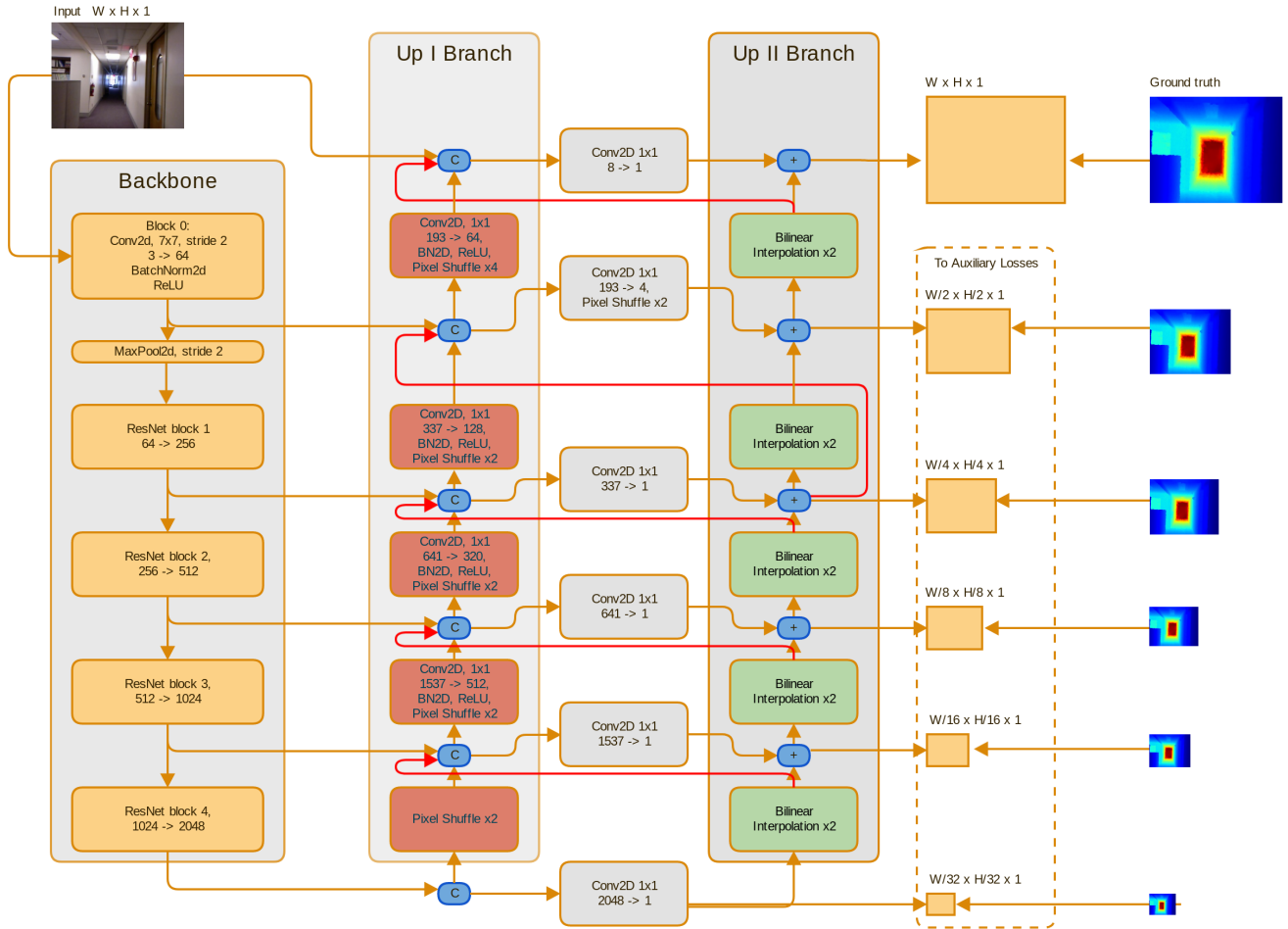


Fig. 1. Double Refinement Network architecture. The downsampling (yellow) branch, represents the backbone. The figure shows ResNet ≥ 50 as a backbone, but the logic for the other pre-trained networks remains the same. The network contains two upsampling branches (red and green). Red branch (up I) merges the high-level features with the low-level features and upsamples them with pixel shuffle. The green branch (up II) outputs intermediate depth maps on each scale, which enables us to compute the loss on every level and supports the training of the lower layers. To propagate the predictions to higher levels, we use bilinear interpolation. The red arrows are referred to as the diagonal connections in the text.

B. Architecture Description

Fig. 1 shows the architecture of the proposed network.

The network consists of one downsampling branch (backbone) and two upsampling branches.

In this paper, we use the following notation: $down_i$ is the output of the down branch on the level i . For the upsampling branches we count from the top, i -th blocks of the upI and upII branches we denote as upI_i and $upII_i$ correspondingly. Besides, $BI(\cdot)$ stands for bilinear interpolation by a factor of 2.

We use a pre-trained backbone network, experimenting with different architectures: ResNet-50, ResNet-152 [7], DenseNet-161 [13] and SENet-154 [12]. We remove the last fully connected layer and its respective average pooling layer from the pre-trained networks.

The backbone network is split into several blocks (layer 0, 1, 2, 3 and 4). Note that the downsample factor of layer 0 is 4, while for the other blocks, except layer 1, it is 2. We denote the output of layer i as $down_{i+1}$.

The upsampling process is similar to U-Net [21] and RefineNet [17]. To start describing it, we substitute $down_5$ with upI_5 for convenience. upI_5 contains the high-level features extracted from the input.

To get the first approximation of the depths $upII_5$ we apply Conv2D 1×1 to upI_5 .

To compute upI_i , we perform the following operations with upI_{i+1} :

- Conv2d 1×1 (except upI_5 block)
- BatchNorm2D (except upI_5)
- ReLU (except upI_5)
- PixelShuffle $\times 2$ (except upI_1 ; for upI_0 - PixelShuffle $\times 4$).

The output is concatenated with $BI(upII_{i+1})$, which is a lightweight operation due to the small size of intermediate outputs.

The second upsampling branch of the network $upII$ is inspired by Fourier Transform. We make a coarse prediction and then, ascending from the bottom to the top, we make

TABLE II

COMPARISON OF OUR NETWORK WITH DIFFERENT BACKBONES AGAINST OTHER NETWORKS. WE SHOULD NOTE THAT WITH THE RESNET-50 BACKBONE OUR NETWORK PERFORMS WORSE THAN THE BASELINE. WE ARE ABLE TO NARROW THIS GAP WITH ARCHITECTURAL CHANGES (SEE EXPERIMENTS IN IV-B).

	RMSE ↓	Log10 ↓	$\delta_{1.25}$ ↓	$\delta_{1.25^2}$ ↑	$\delta_{1.25^3}$ ↑
Lauina et al. [16]	0.573	0.055	0.811	0.953	0.988
Fu et al. [4]	0.509	0.051	0.828	0.965	0.992
Spek et al. [24]	0.687	0.161	0.704	0.917	0.977
Nekrasov et al. [19]	0.565	-	0.790	0.955	0.990
RSIDE [11] ResNet-50 (paper)	0.555	0.054	0.843	0.968	0.991
RSIDE DenseNet-161 (paper)	0.544	0.053	0.855	0.972	0.993
RSIDE SENet-154 (paper)	0.530	0.050	0.866	0.975	0.993
RSIDE SENet-154 (reproduced)	0.574	0.052	0.845	0.967	0.991
(ours) DRNet ResNet-50	0.587	0.061	0.810	0.961	0.990
(ours) DRNet ResNet-152	0.528	0.050	0.866	0.973	0.993
(ours) DRNet DenseNet-161	0.534	0.052	0.865	0.974	0.994
(ours) DRNet SeNet-154	0.527	0.050	0.868	0.975	0.993

corrections to this prediction. Each level increases the side of the output by a factor of 2.

In particular, the depth approximation upII_i is the sum of $BI(\text{upII}_{i+1})$ and the correction term. To compute the latter, we concatenate down_i , $BI(\text{upII}_{i+1})$ and upI_i and apply Conv2D 1×1 to the result.

C. Loss Function

Depth estimation requires not only pixel-wise accuracy but also spatially coherent result. That is the reason why depth estimation models tend to incorporate depth gradient and normals into their loss functions. The loss we use consists of three parts:

$$L_i = l_i^{\text{depth}} + l_i^{\text{grad}} + l_i^{\text{normal}}, \quad (1)$$

$$l_i^{\text{depth}} = \frac{1}{n} \sum_{j=0}^n F(e_j), \quad (2)$$

$$l_i^{\text{grad}} = \frac{1}{n} \sum_{j=0}^n (F(\nabla_x(e_j)) + F(\nabla_y(e_j))), \quad (3)$$

where $F(x) = \ln(x + \alpha)$, $\alpha > 0$ and $e_j = \|d_j - g_j\|_1$ (d and g standing for predicted and ground truth depth maps respectively),

$$l_i^{\text{normal}} = \frac{1}{n} \sum_{j=0}^n \left(1 - \frac{\langle n_j^d, n_j^g \rangle}{\sqrt{\langle n_j^d, n_j^d \rangle} \sqrt{\langle n_j^g, n_j^g \rangle}} \right), \quad (4)$$

with n^d and n^g standing for predicted and ground truth normals correspondingly:

$$n_i^d = [-\nabla_x(d_i), -\nabla_y(d_i), 1]^T, \quad (5)$$

$$n_i^g = [-\nabla_x(g_i), -\nabla_y(g_i), 1]^T. \quad (6)$$

These loss functions are described in-depth in [11], we apply them without changes.

D. Auxiliary Loss Functions

We treat the intermediate output on i -th level as a down-sampled depth map and calculate the loss between it and the target, downsampled to $\frac{1}{2^i}$ of its original size.

Thus, the overall loss function is computed as:

$$L = \sum_{i=0}^5 L_i. \quad (7)$$

We have also tried upsampling the level-specific result using bilinear interpolation and found that it works worse than downsampling the target.

IV. EXPERIMENTS

We conduct our experiments on the NYU Depth v2 dataset. We use the following common metrics to compare our model to the state-of-the-art models:

- Root mean squared error (RMSE):

$$\sqrt{\frac{1}{|N|} \sum_{i \in N} |d_i - g_i|^2} \quad (8)$$

- Threshold (δ):

$$\% \text{ of } d_i \text{ s.t. } \max\left(\frac{d_i}{g_i}, \frac{g_i}{d_i}\right) < t, \quad (9)$$

where $t \in \{1.25, 1.25^2, 1.25^3\}$

Tables II, III show that our proposed architecture achieves results comparable to the baseline while providing up to 35 times faster inference and requiring up to 10 times less memory per image. In real-time scenarios (batch size 1), the inference FPS rate is up to 18 times higher than the baseline's. The visual results can be found in Table I.

A. Implementation details

We train the model using the pre-trained backbone networks from the torchvision package [20]. We use Adam (amsgrad modification) with learning rate 10^{-4} , weight decay 10^{-4} and the default betas.

TABLE III

COMPARISON OF OUR NETWORK WITH DIFFERENT BACKBONES AGAINST OTHER MODELS IN FPS AND MEMORY CONSUMPTION. THE FPS RATES ARE MEASURED USING TESLA P40 GPU. IN THIS TABLE, "BS" STANDS FOR THE BATCH SIZE.

	FPS (BS 1) \uparrow	FPS (max BS) \uparrow	net RAM \downarrow	RAM / img \downarrow
Nekrasov et al. [19]	78	-	-	-
RSIDE ResNet-50 (reproduced)	2	2 (BS 1)	793 Mb	21 Gb
RSIDE DenseNet-161 (reproduced)	1.7	1.7 (BS 1)	853 Mb	22 Gb
RSIDE SENet-154 (reproduced)	1.5	1.5 (BS 1)	1.7 Gb	21.9 Gb
(ours) DRNet ResNet-50	36	69 (BS 36)	757 Mb	2 Gb
(ours) DRNet ResNet-152	25	55 (BS 19)	1067 Mb	2.9 Gb
(ours) DRNet DenseNet-161	17	33 (BS 14)	839 Mb	3.2 Gb
(ours) DRNet SeNet-154	6	13 (BS 9)	1421 Mb	4 Gb

TABLE IV

EXPERIMENTS WITH ADDITIONAL IMPROVEMENTS TO THE ARCHITECTURE

	RMSE	$\delta_{1,25}$	$\delta_{1,25^2}$	$\delta_{1,25^3}$	FPS
DRNet ResNet-50	0.587	0.810	0.961	0.990	36
+ freeze backbone on train	0.588	0.812	0.961	0.990	
+ Guided Filter	0.564	0.836	0.967	0.992	30
+ kernel size 3 in upI-upII	0.582	0.818	0.961	0.991	
+ kernel size 5 in upI-upII	0.579	0.825	0.964	0.990	37
DRNet ResNet-152	0.528	0.866	0.961	0.990	
+ Guided Filter	0.537	0.867	0.973	0.993	
+ kernel size 5 in upI-upII	0.532	0.864	0.973	0.993	

B. More experiments

Table II demonstrates that the accuracy of the ResNet-50-based network is lower than of the architectures with backbones of higher capacity. We experiment with different changes to the ResNet-50-based model with the intention of transferring the improvements to the more capacious architectures. Table IV represents the results of these experiments.

1) *Frozen weights*: We train the model with frozen backbone weights. No improvements are observed in several experimental settings.

2) *Guided Filter*: We substitute bilinear interpolation of intermediate outputs in upII with the Guided Filter upsampling method proposed in [25]. This change provides an increase in accuracy while retaining similar performance.

3) *Correction term layers*: We study the importance of the layers that produce the correction term for the intermediate outputs (grey blocks in Fig. 1). We increase the receptive field of the layers by changing the kernel size. This results in a higher score and does not slow down the inference.

While introducing these changes to the architecture with the ResNet-50 backbone improves the metrics significantly, they do not provide substantial benefits to the models with more capacious backbones.

C. Ablation Studies

We introduce several changes to the baseline. To ensure that each of them contributes to the result, we conduct element reasoning experiments. The results are shown in Table V. From them, we infer that the second upsampling branch

gives the most noticeable improvement. The auxiliary losses slightly improve the metrics, while the diagonal connections appear to have no effect on the result and can be excluded from the network.

TABLE V

RESULTS OF EXPERIMENTS WITH EXCLUSION OF EACH OF THE PROPOSED ELEMENTS FROM DOUBLE REFINEMENT NETWORK WITH THE RESNET-152 BACKBONE.

	RMSE	$\delta_{1,25}$	$\delta_{1,25^2}$	$\delta_{1,25^3}$
DRNet ResNet-152	0.528	0.866	0.972	0.993
no diagonal connections	0.533	0.866	0.973	0.993
no auxiliary losses	0.544	0.860	0.971	0.992
no second branch	1.900	0.351	0.596	0.732

V. CONCLUSIONS

In this paper, we introduced a new architecture for monocular depth estimation. The network works significantly faster and uses 10 times less memory per image compared to the baseline while achieving state-of-the-art quality. It allows real-time inference at up to 36 FPS without network compression. We achieved this by replacing bilinear interpolation of feature maps to the input size with iterative refinement and applying the loss function to the intermediate outputs.

REFERENCES

- [1] L.-C. Chen, G. Papandreou, F. Schroff, and H. Adam. Rethinking atrous convolution for semantic image segmentation. *arXiv preprint arXiv:1706.05587*, 2017.
- [2] L.-C. Chen, Y. Zhu, G. Papandreou, F. Schroff, and H. Adam. Encoder-decoder with atrous separable convolution for semantic image segmentation. In *ECCV*, 2018.
- [3] D. Eigen and R. Fergus. Predicting depth, surface normals and semantic labels with a common multi-scale convolutional architecture. In *Proceedings of the IEEE International Conference on Computer Vision*, pages 2650–2658, 2015.
- [4] H. Fu, M. Gong, C. Wang, K. Batmanghelich, and D. Tao. Deep ordinal regression network for monocular depth estimation. In *Proceedings of the IEEE Conference on Computer Vision and Pattern Recognition*, pages 2002–2011, 2018.
- [5] A. Gupta, M. Hebert, T. Kanade, and D. M. Blei. Estimating spatial layout of rooms using volumetric reasoning about objects and surfaces. In *Advances in neural information processing systems*, pages 1288–1296, 2010.
- [6] A. Gurram, O. Urfalioglu, I. Halfaoui, F. Bouzaraa, and A. M. Lopez. Monocular depth estimation by learning from heterogeneous datasets. *arXiv preprint arXiv:1803.08018*, 2018.

- [7] K. He, X. Zhang, S. Ren, and J. Sun. Deep residual learning for image recognition. In *Proceedings of the IEEE conference on computer vision and pattern recognition*, pages 770–778, 2016.
- [8] L. He, G. Wang, and Z. Hu. Learning depth from single images with deep neural network embedding focal length. *IEEE Transactions on Image Processing*, 2018.
- [9] V. Hedau, D. Hoiem, and D. Forsyth. Thinking inside the box: Using appearance models and context based on room geometry. In *European Conference on Computer Vision*, pages 224–237. Springer, 2010.
- [10] D. Hoiem, A. A. Efros, and M. Hebert. Geometric context from a single image. In *Computer Vision, 2005. ICCV 2005. Tenth IEEE International Conference on*, volume 1, pages 654–661. IEEE, 2005.
- [11] J. Hu, M. Ozay, Y. Zhang, and T. Okatani. Revisiting single image depth estimation: Toward higher resolution maps with accurate object boundaries. 2018.
- [12] J. Hu, L. Shen, and G. Sun. Squeeze-and-excitation networks. 2018.
- [13] G. Huang, Z. Liu, L. Van Der Maaten, and K. Q. Weinberger. Densely connected convolutional networks. In *CVPR*, volume 1, page 3, 2017.
- [14] A. Krizhevsky, I. Sutskever, and G. E. Hinton. Imagenet classification with deep convolutional neural networks. In *Advances in neural information processing systems*, pages 1097–1105, 2012.
- [15] Y. Kuznetsov, J. Stückler, and B. Leibe. Semi-supervised deep learning for monocular depth map prediction. In *Proc. of the IEEE Conference on Computer Vision and Pattern Recognition*, pages 6647–6655, 2017.
- [16] I. Laina, C. Rupprecht, V. Belagiannis, F. Tombari, and N. Navab. Deeper depth prediction with fully convolutional residual networks. In *3D Vision (3DV), 2016 Fourth International Conference on*, pages 239–248. IEEE, 2016.
- [17] G. Lin, A. Milan, C. Shen, and I. D. Reid. Refinenet: Multi-path refinement networks for high-resolution semantic segmentation. In *CVPR*, volume 1, page 5, 2017.
- [18] F. Liu, C. Shen, G. Lin, and I. D. Reid. Learning depth from single monocular images using deep convolutional neural fields. *IEEE Trans. Pattern Anal. Mach. Intell.*, 38(10):2024–2039, 2016.
- [19] V. Nekrasov, T. Dharmasiri, A. Spek, T. Drummond, C. Shen, and I. Reid. Real-time joint semantic segmentation and depth estimation using asymmetric annotations. *arXiv preprint arXiv:1809.04766*, 2018.
- [20] A. Paszke, S. Gross, S. Chintala, G. Chanan, E. Yang, Z. DeVito, Z. Lin, A. Desmaison, L. Antiga, and A. Lerer. Automatic differentiation in pytorch. 2017.
- [21] O. Ronneberger, P. Fischer, and T. Brox. U-net: Convolutional networks for biomedical image segmentation. In *International Conference on Medical image computing and computer-assisted intervention*, pages 234–241. Springer, 2015.
- [22] A. Saxena, M. Sun, and A. Y. Ng. Make3d: Learning 3d scene structure from a single still image. *IEEE transactions on pattern analysis and machine intelligence*, 31(5):824–840, 2009.
- [23] K. Simonyan and A. Zisserman. Very deep convolutional networks for large-scale image recognition. In *International Conference on Learning Representations*, 2015.
- [24] A. Spek, T. Dharmasiri, and T. Drummond. Cream: Condensed real-time models for depth prediction using convolutional neural networks. *arXiv preprint arXiv:1807.08931*, 2018.
- [25] H. Wu, S. Zheng, J. Zhang, and K. Huang. Fast end-to-end trainable guided filter. In *CVPR*, 2018.
- [26] H. Zhao, J. Shi, X. Qi, X. Wang, and J. Jia. Pyramid scene parsing network. In *IEEE Conf. on Computer Vision and Pattern Recognition (CVPR)*, pages 2881–2890, 2017.